Received: 13 April 2024 | Accepted: 13 August 2024

DOI: 10.1002/pamm.202400030

RESEARCH ARTICLE

A finite element framework for thermo-mechanically coupled gradient-enhanced damage formulations

Lennart Sobisch[1] | **Tobias Kaiser**[1] | **Andreas Menzel**[1,2]

[1]Institute of Mechanics, TU Dortmund University, Dortmund, Germany

[2]Division of Solid Mechanics, Lund University, Lund, Sweden

Correspondence
Lennart Sobisch, Institute of Mechanics, TU Dortmund University, Dortmund, Germany.
Email: lennart.sobisch@tu-dortmund.de

Funding information
Deutsche Forschungsgemeinschaft, Grant/Award Number: 278868966

Abstract

The solution of coupled multi-field problems by means of commercially available finite element codes such as Abaqus constitutes an important part in the study of industrial processes. Against this background, a comprehensive implementation framework for a gradient-enhanced continuum damage formulation in a thermo-mechanically coupled finite deformation setting is proposed in this contribution. To assess the applicability of the implementation framework to industrial processes, a thermo-mechanically coupled, gradient-enhanced ductile damage model is exemplarily employed. The resulting three-field problem, consisting of the balance of linear momentum, the heat equation and the balance of micromorphic momentum, is implemented based on an Abaqus user material by making use of a novel two-instance formulation. Representative simulation results are discussed, with the specific focus lying on the application to manufacturing processes involving complex contact interactions. The Abaqus framework is made available as an open-source code on GitHub, see Sobisch et al., Finite Elements in Analysis and Design 232 (2024) 104105.

1 | INTRODUCTION

Characterising damage mechanisms plays an important role in modelling industrial processes, as demonstrated in [1–3] for forming processes. As the manufactured part is typically subjected to large deformations, various damage mechanisms, such as void growth and nucleation, microcracks, and decohesion, significantly affect the properties of the resulting product. Moreover, industrial processes such as extrusion and forging are subject to non-isothermal conditions. Therefore, it is necessary to characterise damage-temperature interactions and to model the process in a thermo-mechanically coupled setting, see for example, [4]. In addition, complex contact interactions between the tool and the component pose an additional challenge for simulation approaches that needs to be addressed. Against this background, this contribution focuses on the implementation of such problems with numerically complex structures, including coupled multiphysics effects, contact problems and material non-linearities, into Abaqus.

In view of the previously described microstructural degradation mechanisms, the development of phenomenological ductile damage models is cardinal to accurately capture the constitutive response of metals in simulations. In Lemaitre-type models, which for the scalar-valued case are also referred to as $[1-d]$ models, effective quantities for the elasticity

and plasticity related contribution of the material model are introduced. However, incorporating these models into the balance of linear momentum results in a loss of ellipticity of the governing partial differential equation and ill-posedness of the related boundary value problems. Gradient-enhancement, respectively the micromorphic approach is commonly used as a regularisation technique in damage formulations to address this issue [5–8].

Modelling damage based on a micromorphic continuum approach in a thermo-mechanically coupled setting results in a system of three coupled partial differential equations. As this contribution focuses on the application of the resulting multi-field framework to manufacturing processes, an implementation into the commercial finite element software Abaqus is aspired. A solution scheme for a user-defined multi-field problem is not available in the standard Abaqus workspace. However, the definition of user elements (UEL) allows for the implementation of an arbitrary number of degrees of freedom. A major drawback of an implementation approach based on user elements is its limited applicability to several built-in Abaqus features, such as various contact algorithms, element formulations and solver structures, see for example, [9]. As an alternative it was suggested in [10, 11] to use the structural similarity of the heat equation and the micromorphic field equation, and to solve the two-field problem based on an Abaqus user material (UMAT). The extension of this approach to arbitrary multi-field problems was proposed in [12] and enables the implementation of the micromorphic approach towards continuum damage mechanics in a thermo-mechanically coupled setting based on user materials.

In view of these developments, the investigation of damage-temperature interactions in forming processes is in the focus of this contribution, with key aspects being:

- A thermo-mechanically coupled, gradient-enhanced damage model.
- The implementation into Abaqus based on user materials.
- The application to a forward rod extrusion process as a benchmark problem for complex forming processes.

2 | CONTINUUM THERMODYNAMICS AND CONSTITUTIVE RELATIONS

2.1 | Micromorphic approach in thermomechanics

Consider a material body, which is subjected to finite deformations, and let the non-linear deformation map $\boldsymbol{\varphi}(\boldsymbol{X}, t)$ relate the position of a material point in the reference configuration $\boldsymbol{X} \in \mathcal{B}_0$ to its position in the spatial configuration $\boldsymbol{x} \in \mathcal{B}_t$. The deformation gradient is defined as $\boldsymbol{F} = \partial\boldsymbol{\varphi}/\partial\boldsymbol{X}$ and $J = \det(\boldsymbol{F}) > 0$, holds. The governing set of partial differential equations for a micromorphic continuum in a thermo-mechanically coupled setting (with micromorphic field variable $\phi(\boldsymbol{X}, t)$ and absolute temperature $\theta(\boldsymbol{X}, t)$) reads

$$\text{balance of linear momentum} \qquad \nabla_{\boldsymbol{X}} \cdot \boldsymbol{P} = \boldsymbol{0} \quad \text{in } \mathcal{B}_0 \tag{1a}$$

$$\text{balance of micromorphic momentum} \qquad \nabla_{\boldsymbol{X}} \cdot \boldsymbol{Y} - Y = 0 \quad \text{in } \mathcal{B}_0 \tag{1b}$$

$$\text{heat equation} \qquad -\nabla_{\boldsymbol{X}} \cdot \boldsymbol{Q} + r = c_0\,\dot{\theta} \quad \text{in } \mathcal{B}_0 \tag{1c}$$

where free energy density Ψ is a potential for Piola stress tensor $\boldsymbol{P}$, micromorphic flux $\boldsymbol{Y}$ and micromorphic source Y, with

$$\boldsymbol{P} = \frac{\partial \Psi}{\partial \boldsymbol{F}}, \quad Y = \frac{\partial \Psi}{\partial \phi}, \quad \boldsymbol{Y} = \frac{\partial \Psi}{\partial \nabla_{\boldsymbol{X}} \phi}\,. \tag{2}$$

The referential heat flux vector can be defined according to Fourier's law with $\boldsymbol{Q} = -K_0\,\nabla_{\boldsymbol{X}}\theta$, whereby K_0 is the conductivity coefficient. Furthermore, the volume-specific heat capacity is given as $c_0 = -\rho_0\,\theta\,\partial^2\Psi/\partial^2\theta$ with referential mass density ρ_0. In general, the heat equation can be derived from the balance of energy, with the volume distributed heat source r taking the form

$$r = \underbrace{\theta\,\frac{\partial \boldsymbol{P}}{\partial \theta} : \dot{\boldsymbol{F}}}_{r^{\mathrm{e}}} + \underbrace{\theta\,\frac{\partial Y}{\partial \theta}\,\dot{\phi} + \theta\,\frac{\partial \boldsymbol{Y}}{\partial \theta} \cdot \nabla_{\boldsymbol{X}}\dot{\phi}}_{r^{\mathrm{mic}}} + \underbrace{D^{\mathrm{red}}_{\mathrm{mech}} - \theta\,\frac{\partial D^{\mathrm{red}}_{\mathrm{mech}}}{\partial \theta}}_{r^{\mathrm{ih}}}, \tag{3}$$

with non-dissipative heat sources r^{e} and r^{mic}, whereas r^{ih} is the dissipative contribution. Therein, the reduced mechanical dissipation is defined as $D^{\mathrm{red}}_{\mathrm{mech}} = -\partial\Psi/\partial\boldsymbol{k} \bullet \dot{\boldsymbol{k}}$ with a set of internal variables $\boldsymbol{k}$.

2.2 | A thermo-mechanically coupled multi-surface ductile damage model

In order to investigate the solution framework for a coupled system of three field equations and to demonstrate its applicability to complex process simulations, a prototype thermo-mechanically coupled gradient-enhanced ductile damage model is briefly discussed in this section. The material model presented is a thermo-mechanically extended version of the isothermal ductile damage model proposed in [13]. An additive decomposition of the energy potential into a local and a non-local part is assumed, namely

$$\Psi(\boldsymbol{F}, \boldsymbol{F}_{\mathrm{p}}, \theta, \phi, \nabla_{\boldsymbol{X}}\phi, d, \alpha) = \Psi^{\mathrm{loc}}(\boldsymbol{F}, \boldsymbol{F}_{\mathrm{p}}, \theta, d, \alpha) + \Psi^{\mathrm{nl}}(\boldsymbol{F}, \phi, \nabla_{\boldsymbol{X}}\phi, d)\,. \tag{4}$$

Therein, $\boldsymbol{F}_{\mathrm{p}}$ is the plastic part of the deformation gradient, with $\boldsymbol{F}_{\mathrm{p}} = \boldsymbol{F}_{\mathrm{e}}^{-1} \cdot \boldsymbol{F}$, α is the accumulated plastic strain and d denotes a local damage variable, characterising the degradation of the material. The non-local contribution is based on the seminal works [5, 6] and reads

$$\Psi^{\mathrm{nl}}(\boldsymbol{F}, \phi, \nabla_{\boldsymbol{X}}\phi, d) = \frac{c_d}{2}\,\|\nabla_{\boldsymbol{X}}\phi\|^2 + \frac{\beta_d}{2}\,[\phi - d]^2\,, \tag{5}$$

where regularisation parameter c_d weights the gradient of the micromorphic damage variable and where β_d is a penalty parameter which enforces the coupling between the local and the micromorphic damage fields. A split of the energy potential is assumed, that is,

$$\Psi^{\mathrm{loc}}(\boldsymbol{F}, \boldsymbol{F}_{\mathrm{p}}, \theta, d, \alpha) = f^{\mathrm{vol}}(d)\,\Psi^{\mathrm{vol}}(\boldsymbol{F}_{\mathrm{e}}, \theta) + f^{\mathrm{iso}}(d)\,\Psi^{\mathrm{iso}}(\boldsymbol{F}_{\mathrm{e}}) + \Psi^{\mathrm{cal}}(\theta) + \Psi^{\mathrm{p}}(\alpha)\,, \tag{6}$$

with different damage functions $f^{\bullet}(d) = \exp(-\eta_{\bullet}\, d)$ acting on the volumetric and isochoric contributions. Thereby, material parameters $\eta_{\bullet}$ characterise the degradation of the respective energy contributions. In addition, the local energy contains a caloric and a hardening contribution. The energy potentials considered are specified as

$$\Psi^{\mathrm{vol}}(\boldsymbol{F}_{\mathrm{e}}, \theta) = \frac{1}{2}\,\lambda\,\ln(J_{\mathrm{e}})^2 - \ln(J_{\mathrm{e}})\,\left[\mu + 3\,\alpha_\theta\,K\,[\theta - \theta_0]\,J_{\mathrm{e}}^{-1}\right]\,, \quad \Psi^{\mathrm{iso}}(\boldsymbol{F}_{\mathrm{e}}) = \frac{1}{2}\,\mu\,[\boldsymbol{F}_{\mathrm{e}} : \boldsymbol{F}_{\mathrm{e}} - 3]\,, \tag{7a-b}$$

$$\Psi^{\mathrm{cal}}(\theta) = \bar{c}_0\,\left[\theta - \theta_0 - \theta\,\ln\left(\theta\,\theta_0^{-1}\right)\right]\,, \qquad \Psi^{\mathrm{p}}(\alpha) = \frac{h}{n_{\mathrm{p}} + 1}\,\alpha^{n_{\mathrm{p}}+1}\,, \tag{7c-d}$$

with Lamé parameters λ, μ, bulk modulus $K = \lambda + 2\,\mu/3$ and thermal expansion coefficient α_θ. The caloric contribution is characterised by the heat capacity coefficient $\bar{c}_0$, while h and n_{p} control the non-linear hardening behaviour. Following the Coleman and Noll procedure yields the reduced mechanical dissipation inequality

$$\mathcal{D}_{\mathrm{mech}}^{\mathrm{red}} = \boldsymbol{M}_{\mathrm{e}} : \boldsymbol{L}_{\mathrm{p}} + \beta\,\dot{\alpha} + q\,\dot{d}\,, \tag{8}$$

where $\boldsymbol{L}_{\mathrm{p}} = \dot{\boldsymbol{F}}_{\mathrm{p}} \cdot \boldsymbol{F}_{\mathrm{p}}^{-1}$ is the plastic velocity gradient. The thermodynamic driving forces, to be more specific the (intermediate) Mandel stresses $\boldsymbol{M}_{\mathrm{e}}$, the isotropic hardening stress β and the damage driving force q follow as

$$\boldsymbol{M}_{\mathrm{e}} = \boldsymbol{F}_{\mathrm{e}}^{\mathrm{t}} \cdot \frac{\partial \Psi}{\partial \boldsymbol{F}_{\mathrm{e}}}, \quad \beta = -\frac{\partial \Psi}{\partial \alpha}, \quad q = -\frac{\partial \Psi}{\partial d}\,. \tag{9}$$

A multi-surface formulation is employed based on the potentials

$$\Phi_{\mathrm{p}}(\boldsymbol{M}_{\mathrm{e}}, \beta, d, \theta) = \left\|\mathrm{dev}\left(\frac{\boldsymbol{M}_{\mathrm{e}}}{f^{\boldsymbol{M}_{\mathrm{e}}}(d)}\right)\right\| - \sqrt{\frac{2}{3}}\,\left[\sigma_y(\theta) - \beta\right]\,, \tag{10a}$$

$$\Phi_d(q, d, \alpha) = \frac{H(J-1)\,q}{f^{\alpha}(\alpha)} - q^{\max}\,[1 - f^{q}(d)]^{n_d} - q^{\min}\,, \tag{10b}$$

where $\sigma_y(\theta)$ is the temperature dependent yield limit and $q^{\min}$ ($q^{\max}$) is the minimum (maximum) threshold value for the damage driving force. Due to the significant tension-compression asymmetry of the damage evolution in metals, the

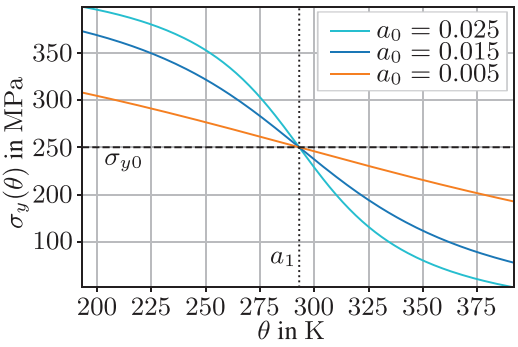

FIGURE 1 Visualisation of yield limit $\sigma_y(\theta)$ as a function of temperature θ.

TABLE 1 Material parameters for the thermal contributions of the constitutive model.

Material parameter	Symbol	Reference	Lower	Upper	Unit
Heat capacity	$\bar{c}_0$	2.0	—	—	mJ/gK
Thermal expansion	α_θ	$1 \cdot 10^{-5}$	—	—	K^{-1}
Yield limit coeff.	a_0	0.015	—	—	K^{-1}
Reference temperature	a_1	293	—	—	K
Initial temperature	θ_0	343	293	393	K

Note: The mechanical properties have been identified for 16MnCrS5 in ref. [14].

Heaviside function H is incorporated so that damage evolution under compressive states is neglected. The temperature dependent yield limit is assumed to take the form

$$\sigma_y(\theta) = \frac{\sigma_{y0}}{2} \left[\arctan(-a_0 \left[\theta - a_1\right]) + 2\right], \tag{11}$$

and is visualised in Figure 1. Therein, σ_{y0} denotes the initial yield stress at reference temperature a_1. Invoking the postulate of maximum dissipation yields evolution equations for the internal variables and the respective Karush-Kuhn Tucker conditions which are enforced by making use of a Fischer-Burmeister approach. Based on (3), the volume distributed heat source can be additively decomposed as $r = r^{\mathrm{e}} + r^{\mathrm{mic}} + r^{\mathrm{p}} + r^{d}$ with

$$r^{\mathrm{e}} = \theta \frac{\partial \boldsymbol{P}}{\partial \theta} : \dot{\boldsymbol{F}}, \quad r^{\mathrm{p}} = \boldsymbol{M}_{\mathrm{e}} : \boldsymbol{L}_{\mathrm{p}} + \beta\, \dot{\alpha} - \theta \frac{\partial \boldsymbol{M}_{\mathrm{e}}}{\partial \theta} : \boldsymbol{L}_{\mathrm{p}}, \quad r^{d} = q\, \dot{d} - \theta \frac{\partial f^{\mathrm{vol}}}{\partial d} \frac{\partial \Psi^{\mathrm{vol}}}{\partial \theta} \dot{d}\,. \tag{12}$$

Due to the temperature independence of the micromorphic quantities $\boldsymbol{Y}$ and Y, the micromorphic heat source vanishes ($r^{\mathrm{mic}} = 0$). In the ensuing numerical investigations, the material parameters determined in [14] for the case hardening steel 16MnCrS5 are employed. Furthermore, the thermal parameters of the model are chosen as summarised in Table 1.

3 | FINITE ELEMENT FRAMEWORK AND ABAQUS IMPLEMENTATION

This section briefly discusses the finite element framework based on Abaqus user materials. As summarised in (1), the proposed micromorphic approach in a thermo-mechanical setting requires the solution of a coupled set of three partial differential equations. The finite element software Abaqus provides two implementation options for user-defined multi-field problems. A highly customisable strategy is the definition of user elements which require the specification of the local element formulation and are therefore not limited to a specific number of degrees of freedom. A major drawback of user elements is their incompatibility with many built-in Abaqus features, such as various contact algorithms, solver structures and structural elements. This makes the implementation of user elements impractical for many appli-

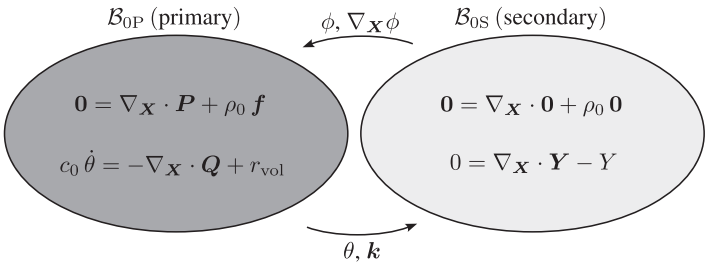

FIGURE 2 Allocation of the three-field problem onto two domains according to [12].

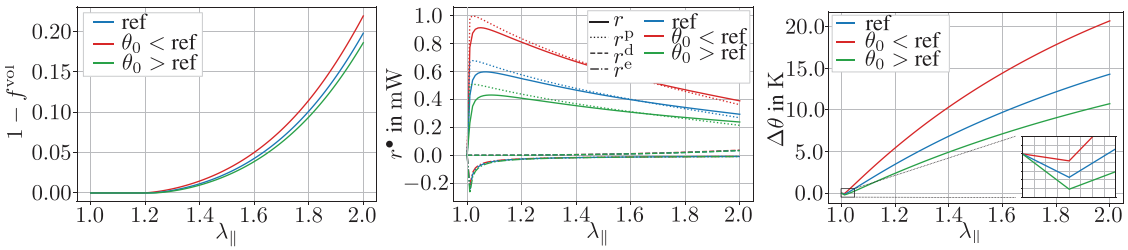

FIGURE 3 Evolution of constitutive quantities for uniaxial stress state with axial stretch $\lambda_\parallel$.

cations, such as the simulation of complex manufacturing processes involving sophisticated contact interactions. The second implementation strategy for custom multi-field problems is based on user materials. Although compatible with many built-in Abaqus features, classic user materials are unfortunately limited to the implementation of two-field problems. An extension of user materials to a specific class of multi-field problems was proposed in [12] and will be used in this paper. The basic idea of the implementation framework is to split the three-field problem onto two domains, as illustrated in Figure 2. Consequently, the balance of linear momentum and the heat equation are solved on the primary domain, whereas the micromorphic field equation and a zero-valued balance equation are solved on the secondary domain. A coupling of both domains is enforced by applying linear constraints to the mechanical degrees of freedom so that the secondary instance acts as a follower domain to the primary instance. In general, the implementation framework leads to a loss of quadratic convergence [12]. In the following, the solution strategy will be referred to as the two-instance approach.

4 | NUMERICAL EXAMPLES

4.1 | Uniaxial tensile stress state

A single element test is performed to demonstrate the characteristics of the implemented ductile damage model. The hexagonal Abaqus element `C3D8T` is subjected to uniaxial stress states so that the constitutive model can be evaluated at a material point level. The considered boundary value problem leads to a homogeneous distribution of the micromorphic damage variable. Consequently, the regularisation characteristics of the model cannot be assessed for this problem. For the thermal problem, adiabatic boundary conditions are assumed and the initial temperature of the element is varied in the following investigations.

To evaluate the material model, the volumetric damage function $1 - f^{\mathrm{vol}}$, the heat source contributions $r^\bullet$ and the temperature change are visualised in Figure 3 for different initial temperatures. The elastic energy is lower for a higher initial temperature compared to the reference solution due to the decrease of yield limit $\sigma_y(\theta)$ with temperature. As the driving force for damage evolution is directly correlated to the elastic energy, damage evolution decreases with increasing temperature. Focusing on the different contributions to the heat source, it can be observed that the internal heat generation is dominated by plastic deformations. The damage related heat source has the least influence on the temperature evolution.

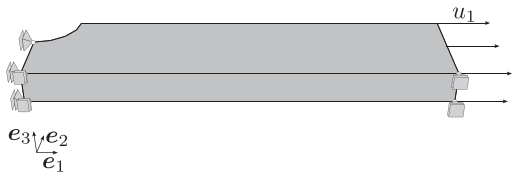

FIGURE 4 Visualisation of the three-dimensional notched plate test. Dirichlet boundary conditions are applied according to the symmetry planes of the specimen.

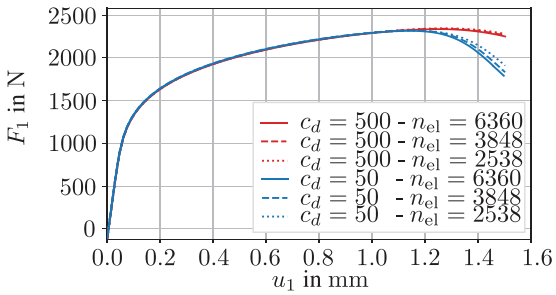

FIGURE 5 Force-displacement curve for different finite element discretisations.

For this particular model, a decrease in the initial temperature results in an increase in the heat source due to higher stress levels.

4.2 | Notched plate test

In order to demonstrate the mesh-objectivity of the gradient-enhanced damage model, a notched plate under tension (length 20.0 mm, height 5.0 mm, thickness 1.5 mm, notch radius 2.0 mm) is investigated, as visualised in Figure 4. Due to the symmetry of the problem, only a quarter of the plate with appropriated symmetry boundary conditions is considered.

The specimen is loaded displacement driven in $\boldsymbol{e}_1$ direction. Adiabatic boundary conditions and the initial condition $\theta_0 = 343$ K are assumed for the thermal problem. Furthermore, homogeneous Neumann boundary conditions are applied for the micromorphic field variable. The underlying finite element problem is solved using Abaqus `C3D8T` elements, where the number of elements $n_{\mathrm{el}} \in \{2538, 3848, 6360\}$ is varied in order to investigate the mesh objectivity of the results. In addition to the element size, the regularisation parameter c_d is varied with $c_d \in \{50, 500\}$ N.

The reaction force in $\boldsymbol{e}_1$ direction is visualised in Figure 5 as a function of elongation. For all three finite element meshes, the global reaction force qualitatively coincides. However, a sufficient number of elements is required to achieve convergence upon mesh refinement for a small regularisation parameter c_d since the localised deformation zone needs to be properly resolved. Contour plots for the volumetric damage contribution $1 - f^{\mathrm{vol}}(d)$, the temperature change $\Delta\theta$, the 11-coefficient of plastic deformation gradient $F_{\mathrm{p},11}$ and for the heat source r are visualised in Figure 6. The regularisation parameter c_d weights the gradient of the micromorphic damage variable and thus directly influences the localisation zone. Due to the rather small influence of the damage related heat source on the total heat generation, the influence of the regularisation parameter on the temperature evolution is not significant for the considered problem.

4.3 | Forward rod extrusion

A forward rod extrusion process is exemplarily studied in this section as the main objective of the finite element framework based on the two-instance formulation and the corresponding Abaqus implementation is to enable the study of manufacturing processes with sophisticated non-local damage models. The process geometry is based on [15] and visualised in Figure 7. Due to the radial symmetry of the process, only a planar section with appropriate symmetry boundary conditions is considered. The extruded part is modelled as a deformable body with the gradient-enhanced ductile damage model of Section 2.2 being invoked, and with adiabatic boundary conditions being considered. The die is modelled as an isothermal

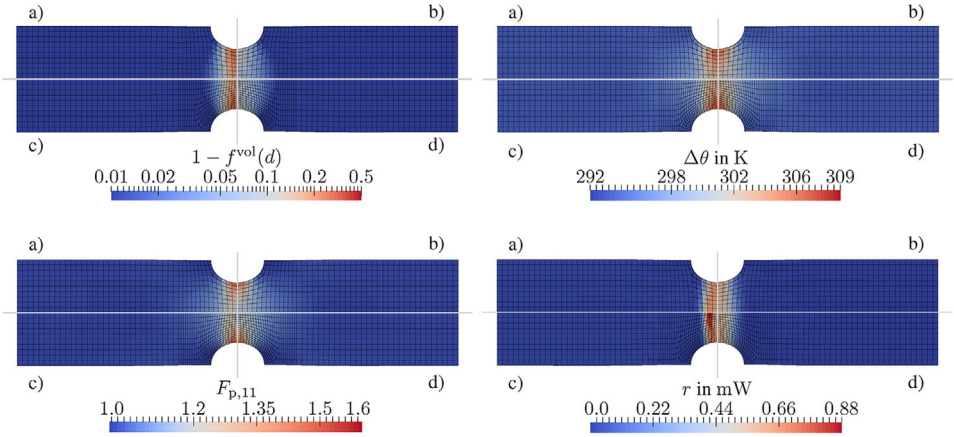

FIGURE 6 Volumetric damage function, temperature change, plastic deformation gradient and heat source for a coarse (a, b) and a fine (c, d) finite element discretisation and regularisation parameters $c_d = 50\,\mathrm{N}$ (a, c) and $c_d = 500\,\mathrm{N}$ (b, d).

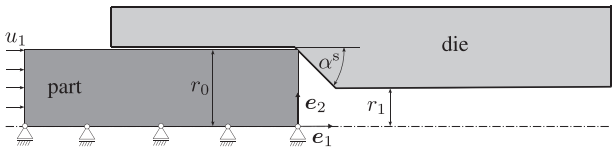

FIGURE 7 Visualisation of the analysed radially-symmetric extrusion process. Dirichlet boundary conditions are applied according to the symmetry planes of the coordinate system.

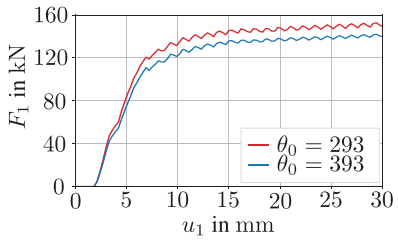

FIGURE 8 Reaction force in $\boldsymbol{e}_1$ direction as a function of prescribed displacement u_1 for different initial temperatures.

rigid body. The initial condition for the deformable part is varied for the investigations, with $\theta_0 \in \{293, 393\}\,\mathrm{K}$. An Augmented Lagrange approach together with the *general contact* algorithm available in Abaqus [16] is used to account for the normal contact interaction between the two bodies. For the tangential contact interaction, a friction coefficient $\mu^{\mathrm{fr}} = 0.04$ is assumed. The horizontal displacement u_1 is prescribed on the left boundary of the deformable part to induce a relative translation between both bodies. For the following investigations, the initial radius $r_0 = 15\,\mathrm{mm}$, the extrusion strain $\varphi^{\mathrm{extr}} = 2\,\ln(r_0/r_1) = 0.3$ and the shoulder opening angle $2\,\alpha^{\mathrm{s}} = 30^\circ$ have been chosen. The underlying finite element problem is solved with axis-symmetric `CAX4HT` elements and an implicit time integration scheme.

As depicted in Figure 8, a higher initial temperature results in a lower maximum process force, due to the decrease in yield limit with increasing temperature. Contour plots for the volumetric damage contribution $1 - f^{\mathrm{vol}}(d)$, the stress triaxiality $\eta^{\mathrm{triax}} = \sqrt{2}\,\mathrm{tr}(\boldsymbol{\sigma})/\sqrt{27}\,\|\mathrm{dev}(\boldsymbol{\sigma})\|$ with the Cauchy stresses $\boldsymbol{\sigma} = J_{\mathrm{e}}^{-1}\,[\boldsymbol{F}_{\mathrm{e}}^{-\mathrm{t}} \cdot \boldsymbol{M}_{\mathrm{e}} \cdot \boldsymbol{F}_{\mathrm{e}}^{\mathrm{t}}]$, the yield limit $\sigma_y(\theta)$ and the temperature change $\Delta\theta$ are provided in Figure 9. A characteristic of the forward rod extrusion process is the positive stress triaxiality along the centre axis for moderate extrusion strains $\varphi^{\mathrm{extr}} < 0.5$, see [2]. For the proposed material model this leads to damage evolution along the centre axis. Furthermore, damage evolution can be observed in the vicinity of the contact surface where tensile stresses are induced by the frictional interaction of the two bodies. For the model under consideration, a higher initial temperature leads to lower damage evolution in the entire sample as a result of the lower yield strength.

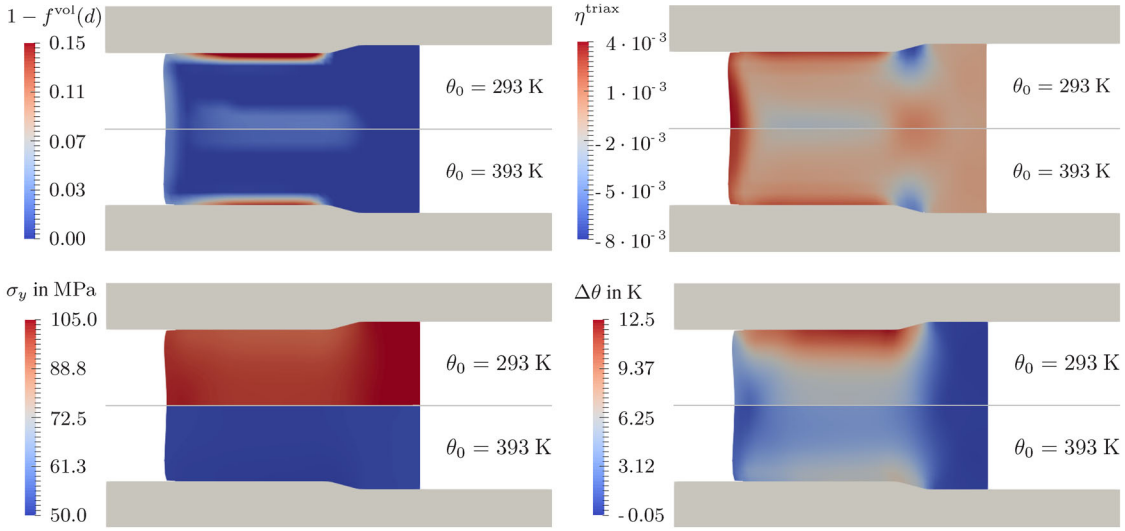

FIGURE 9 Contour plots for the forward rod extrusion process. The volumetric damage contribution, the stress triaxiality, the temperature dependent yield stress and the temperature change are visualised for two different initial temperatures θ_0.

5 | CONCLUSION

Driven by the goal to apply sophisticated multi-field formulation in the simulation of manufacturing processes, an Abaqus user material framework for a system of three coupled field equations was presented. In order to assess the applicability of the provided framework, a thermo-mechanically coupled and gradient-enhanced ductile damage model was discussed and applied to study representative boundary value problems. Amongst others, the simulation of a forward rod extrusion process with complex contact interactions was performed. The solution of the corresponding three-field problem was obtained for different initial temperatures, with lower initial temperatures leading to higher maximum damage values at the locations of positive stress triaxiality. An experimental verification of the simulation results for the considered extrusion process will be the focus of future works.

ACKNOWLEDGMENTS

Funded by the Deutsche Forschungsgemeinschaft (DFG, German Research Foundation) – Project-ID 278868966 – TRR 188.
Open access funding enabled and organized by Projekt DEAL.

ORCID

Lennart Sobisch https://orcid.org/0000-0001-7483-5113
Tobias Kaiser https://orcid.org/0000-0002-1979-1944
Andreas Menzel https://orcid.org/0000-0002-7819-9254

REFERENCES

1. Gitschel, R., Hering, O., Schulze, A., & Erman Tekkaya, A. (2022). Controlling damage evolution in geometrically identical cold forged parts by counterpressure. *Journal of Manufacturing Science and Engineering*, *145*(1), 011011.
2. Hering, O., Dunlap, A., Tekkaya, A., Aretz, A., & Schwedt, A. (2020). Characterization of damage in forward rod extruded parts. *International Journal of Material Forming*, *13*(64), 1003–1014.
3. Tekkaya, A., Bouchard, P. O., Bruschi, S., & Tasan, C. (2020). Damage in metal forming. *CIRP Annals*, *69*(2), 600–623.
4. Felder, S., Kopic-Osmanovic, N., Holthusen, H., Brepols, T., & Reese, S. (2022). Thermo-mechanically coupled gradient-extended damage-plasticity modeling of metallic materials at finite strains. *International Journal of Plasticity*, *148*, 103142.
5. Forest, S. (2009). Micromorphic approach for gradient elasticity, viscoplasticity, and damage. *Journal of the Engineering Mechanics*, *135*(3), 117–131.
6. Dimitrijevic, B. J., & Hackl, K. (2008). A method for gradient enhancement of continuum damage models. *Technical Mechanics*, *28*(1), 43–52.
7. Steinmann, P. (1999). Formulation and computation of geometrically non-linear gradient damage. *International Journal for Numerical Methods in Engineering*, *46*(5), 757–779.

8. Brepols, T., Wulfinghoff, S., & Reese, S. (2020). A gradient-extended two-surface damage-plasticity model for large deformations. *International Journal of Plasticity*, *129*, 102635.
9. Waffenschmidt, T., Polindara, C., Menzel, A., & Blanco, S. (2014). A gradient-enhanced large-deformation continuum damage model for fibre-reinforced materials. *Computer Methods in Applied Mechanics and Engineering*, *268*, 801–842.
10. Ostwald, R., Kuhl, E., & Menzel, A. (2019). On the implementation of finite deformation gradient-enhanced damage models. *Computational Mechanics*, *64*(3), 847–877.
11. Seupel, A., Hütter, G., & Kuna, M. (2018). An efficient fe-implementation of implicit gradient-enhanced damage models to simulate ductile failure. *Engineering Fracture Mechanics*, *199*, 41–60.
12. Sobisch, L., Kaiser, T., Furlan, T., & Menzel, A. (2024). A user material approach for the solution of multi-field problems in Abaqus: Theoretical foundations, gradient-enhanced damage mechanics and thermo-mechanical coupling. *Finite Elements in Analysis and Design*, *232*, 104105.
13. Sprave, L., & Menzel, A. (2020). A large strain gradient-enhanced ductile damage model: finite element formulation, experiment and parameter identification. *Acta Mechanica*, *231*(12), 1–34.
14. Schulte, R., Karca, C., Ostwald, R., & Menzel, A. (2023). Machine learning-assisted parameter identification for constitutive models based on concatenated loading path sequences. *European Journal of Mechanics - A/Solids*, *98*, 104854.
15. Lange, K., Kammerer, M., Pöhlandt, K., & Schöck, J. (2007). *Fließpressen - Wirtschaftliche Fertigung metallischer Präzisionswerkstücke*. Springer.
16. Smith, M. (2009). ABAQUS/Standard User's Manual, Version 6.9. Dassault Systèmes Simulia Corp, United States.

How to cite this article: Sobisch, L., Kaiser, T., & Menzel, A. (2024). A finite element framework for thermo-mechanically coupled gradient-enhanced damage formulations. *Proceedings in Applied Mathematics and Mechanics*, *24*, e202400030. https://doi.org/10.1002/pamm.202400030